Structure and Mechanism of Photooxidation of Self-assembled Monolayers of Alkylthiols on Silver Studied by XPS and Static SIMS

David A. Hutt, Elaine Cooper, and Graham J. Leggett*

Department of Materials Engineering and Materials Design, The University of Nottingham, University Park, Nottingham NG7 2RD, U.K.

Received: July 23, 1997; In Final Form: October 16, 1997[⊗]

XPS and static SIMS have been employed to characterize the structures and the photooxidation of self-assembled monolayers (SAMs) of alkylthiols on silver. Samples were prepared by immersing silver substrates in thiol solutions for a range of times from 30 min to 40 h, but no changes were observed in either the compositions of the monolayers determined by XPS or the static SIMS spectra. Static SIMS spectra exhibited a range of characteristic molecular species that facilitated quantification of changes in the SAM structure following exposure to UV light. Photooxidation led to the formation of alkylsulfonate species at a rate that depended on the length of the adsorbate alkyl chain. However, evaluation of XPS compositional data suggested that significant amounts of unoxidized sulfur remain even when SIMS data indicate the absence of intact, unoxidized thiolate species in the monolayer. In agreement with the results of other workers, we propose that photoirradiation of SAMs on silver leads to two processes: photooxidation of thiol adsorbates to alkylsulfonates and sulfur−carbon bond scission. The latter process, not observed in an earlier study of SAMs on Au, leads to the formation of significant quantities of inorganic sulfur that are subsequently slowly oxidized to yield inorganic oxides of sulfur.

Introduction

Recent years have seen an explosion of interest in self-assembled monolayers (SAMs), including, in particular, monolayers of alkylthiols on gold and silver. These materials have found applications in fundamental studies of a broad range of interfacial phenomena, including wetting and biological interactions. Studies of the wetting properties of SAMs on gold and silver have determined that they exhibit very similar behavior, with monolayers formed from the same alkylthiols yielding similar contact angles.[1] Given that the lattice spacings of the Ag(111) and Au(111) substrates are almost identical, this might be expected. However, STM and X-ray and He atom diffraction studies[2−4] have revealed that the adsorbates adopt a different packing arrangement on the surfaces of the two metals. For SAMs on gold, a commensurate $(\sqrt{3} \times \sqrt{3})R30°$ structure, with a $c(4 \times 2)$ superlattice, has been identified,[5−7] while for SAMs on Ag, the structure appears to be different and may be incommensurate. As a result of this, thiols exhibit different tilt angles on silver and gold (respectively, 12° and 27° relative to the surface normal for SAMs on Ag and Au) and the packing densities are different (19.1 and 21.6 Å^2/chain respectively[8,9]). In early work on the formation of SAMs on Ag, Whitesides and co-workers[8] noticed an increase in the S XPS signal from the monolayer with extended exposure time to the thiol solution, leading to a value far in excess of that expected for a single layer of thiol molecules on the surface. They attributed this to the formation of a silver sulfide interlayer, and it may be this structure that results in the different arrangement of the molecules on the silver surface.

The discovery of patterning techniques for the production of surfaces with spatially well-defined regions of different chemical functionality has further fueled the interest in SAMs as they present opportunites to direct the attachment of molecules and biological species at specific areas of the surface leading to the preparation of microstructured arrays with applications in sensors and molecular electronics. A number of patterning procedures have been devised, including microcontact printing,[10−13] micromachining,[14] and photolithography.[15−18] The photolithographic procedure is relatively simple and involves the exposure of the monolayer in air to UV light through a mask, photooxidizing the thiolate species in the exposed regions. Photooxidation is thought to result in the formation of alkylsulfonate groups ($R-SO_3$).[15−17,19,20] This species is only weakly bound to the Au substrate and can be readily displaced from the surface by another thiol molecule adsorbed from solution, producing a patterned surface. In an earlier study, we examined the rate of the photooxidation process for SAMs on gold as a function of alkyl chain length.[20] We showed that SAMs formed from long-chain molecules were photooxidized more slowly than those containing molecules with short chains, a consequence of the greater order in the long-chain molecules preventing the penetration of the oxidizing species to the S−Au interface. On Ag an alternative mechanism has been proposed by Lewis et al.[21] On the basis of Raman spectroscopy data, they suggested that photooxidation involved the scission of the S−C bond followed by desorption of the alkyl chain and, subsequently, oxidation of exposed S at the Ag surface. The chain-length dependence of the photooxidation rate derived from these data was similar to that found in our study of SAMs on gold. However, they attributed this to the increased van der Waals interactions between long chains, holding them at the surface after the S−C scission preventing access of O to the bare S.

* To whom correspondence should be addressed. E-mail: Graham.Leggett@Nottingham.ac.uk.

[⊗] Abstract published in *Advance ACS Abstracts,* December 15, 1997.

S1089-5647(97)02394-8 CCC: $15.00
Published on Web 01/01/1998

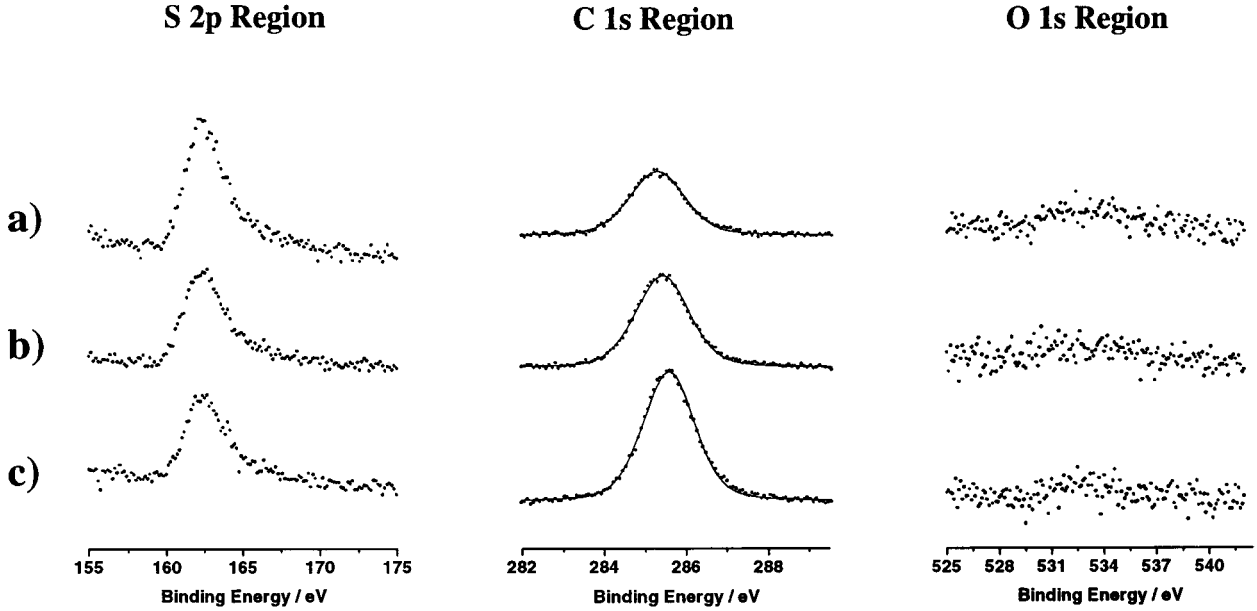

Figure 1. S $2p_{(3/2,1/2)}$, C 1s, and O 1s XPS spectra of freshly prepared SAMs of (a) octanethiol, (b) dodecanethiol, and (c) octadecanethiol on silver.

In the present study we have used XPS and static SIMS to examine the photooxidation of SAMs of alkylthiols adsorbed onto evaporated silver surfaces. We have compared our data with expectations based on the model of Lewis et al.[21] and with our previous findings for SAMs on Au.[20] In addition, we have also determined the nature of any effects that might be due to the presence of a sulfide interlayer between the SAM and the substrate.

Experimental Section

Sample Preparation. SAMs of methyl-terminated molecules were formed on evaporated silver films supported on glass coverslips. The silver was deposited at a rate of ~0.3 Å s^{-1} to a thickness of ~250 Å in a diffusion-pumped bell jar vacuum system with a base pressure of $<1 \times 10^{-6}$ Torr. The glass substrates (Chance No. 2 thickness) and all other glassware used in the sample preparation were first cleaned by immersion in hot (~90 °C) "Piranha" solution[22] for 30 min before rinsing with copious quantities of reverse osmosis water and drying in an oven at 70 °C. Following evaporation, the silver films were allowed to cool in vacuum before the system was vented with N_2 gas and the slides placed immediately into the adsorption solutions. The thiol compounds used in this study (propanethiol (>97%), hexanethiol (~97%), octanethiol (>97%), decanethiol (>95%), dodecanethiol (>97%), and octadecanethiol (~95%)) were all obtained from Fluka and used without further purification. Solutions of the adsorbates (1 mM) in degassed ethanol (99.7%) were prepared immediately before use. Following exposure to the solution for the desired time period, the samples were removed, rinsed with degassed ethanol, and dried with a stream of N_2 gas. Slides for XPS and SIMS analysis were cut into smaller pieces using a diamond-tipped scribe.

Photooxidation of SAMs. Freshly prepared monolayers were photooxidized using a medium pressure mercury arc lamp. This lamp has a warm-up period of approximately 4 min, and UV exposure times quoted here have been corrected for this. Samples were placed face up underneath the lamp approximately 100 mm away from the source and irradiated for the desired period of time. To correlate results taken with SIMS and XPS, several samples were exposed simultaneously and were transferred immediately to the vacuum systems for XPS or SIMS analysis.

XPS Analysis. XPS analysis of samples was conducted in a Vacuum Generators ESCALAB instrument equipped with an unmonochromated twin anode (Mg and Al) X-ray source and 100 mm radius hemispherical electron energy analyzer. Al Kα radiation was used throughout to obtain the spectra with the electron energy analyzer operated in fixed transmission mode. Several different regions of the spectrum were examined in detail using different analyzer pass energies to produce either good resolution or high sensitivity. A survey scan was recorded first followed by C 1s (10 eV pass energy—high resolution), O 1s (20 eV pass energy), S $2p_{(3/2,1/2)}$ (50 eV pass energy—high sensitivity), and Ag $3d_{(7/2,5/2)}$ regions (10, 20, and 50 eV pass energy) for comparison. To avoid sample damage during data collection, the X-ray source was retracted as far from the surface as possible and the number of scans for each spectrum limited to reduce the data collection time.

SIMS Analysis. Static SIMS spectra were recorded on a Vacuum generators instrument using a Ga metal ion gun and MM12-12 quadrupole mass spectrometer. A primary particle energy of 10 keV was used throughout to obtain both positive and negative ion spectra, with the primary ion current of the order of 5 nA cm^{-2}. Primary particle doses were kept below 10^{13} ions cm^{-2}, thereby remaining in the static SIMS regime.

Results

Examination of As-Prepared SAMs on Silver. Methyl-terminated monolayers of different alkyl chain length were prepared on silver surfaces and examined by XPS and SIMS.

Figure 1 shows S $2p_{(3/2,1/2)}$,[24] C 1s, and O 1s regions of the XPS spectrum for monolayers of octanethiol, dodecanethiol, and octadecanethiol prepared by exposure to the adsorption solution for 16 h. For all three SAMs the C 1s peak is symmetrical and can be fitted with a single component, indicating a pure monolayer composition. The peak position shifts slightly to higher BE with increasing C chain length, indicating some charging within the longer monolayers. The size of the C 1s peak increases with increasing C chain length, as expected, and

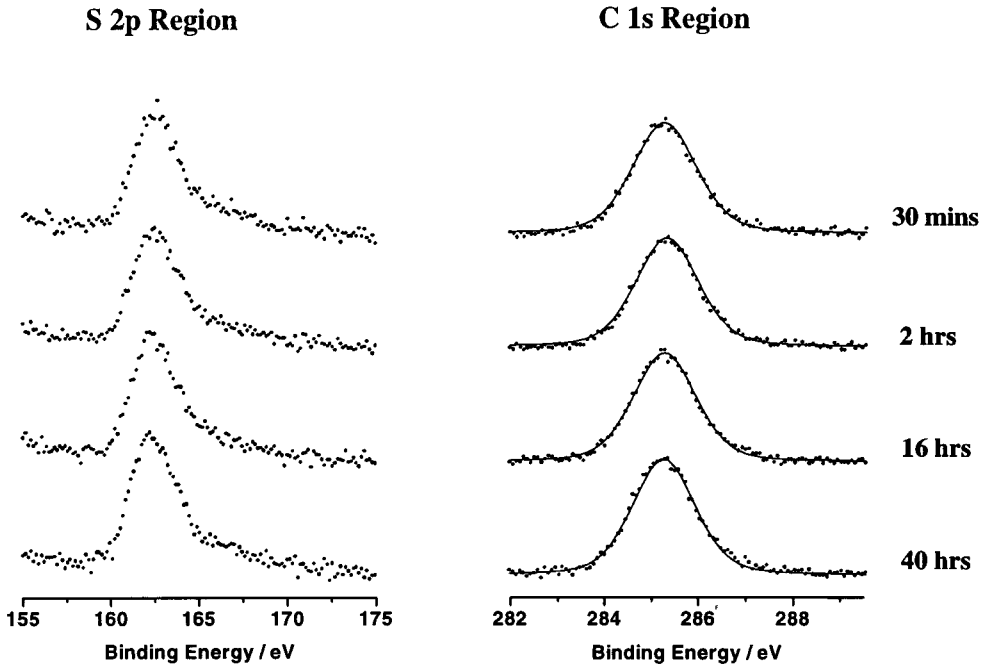

Figure 2. Effect of extended adsorption solution exposure on S $2p_{(3/2,\ 1/2)}$ and C 1s XPS spectra for octanethiol. Times shown indicate the period for which the silver substrate was left in solution before removal, rinsing, and drying.

similarly, the S 2p peaks are attenuated to a greater extent by the longer chain monolayers supporting the picture of the S headgroups adsorbed at the silver surface. All three SAMs show a small contribution from O 1s at 532 eV. This may indicate some contamination within the monolayers and/or oxidation of the silver substrate, an expected process caused by the brief exposure of the silver film to air before immersion in the thiol solution. O was present in the monolayers of Laibinis et al.[8] and could not be excluded completely.

To explore further the possibility that a sulfide interlayer forms during the adsorption of alkylthiols onto silver surfaces, samples were prepared by exposure of the substrate to the preparation solution for a range of periods of time. In Figure 2 the S 2p and C 1s regions of the XPS spectra are shown for SAMs of octanethiol prepared by exposure to the adsorption solution for periods ranging from 30 min to 40 h. It is apparent from these data that there is little change in the quantity of S present on the surface with increasing exposure to the thiol solution. In addition, there has been no change in the quantity of C adsorbed at the surface, with the C 1s peak remaining symmetrical, indicating that only a single layer of thiol has been deposited. This trend of unchanging S and C composition with solution exposure time was also found to occur for SAMs of dodecanethiol and octadecanethiol (data not shown), in contrast to the results of Laibinis et al.[8] who observed an extensive increase in the S content in their SAMs over similar periods in solution.

Positive and negative ion static SIMS spectra were also recorded for samples that had been exposed to solutions of their respective thiols for a range of times. In agreement with the XPS results, the spectra were not observed to change with increasing exposure to the thiol solution and were essentially similar for monolayers of all three thiols.

In the positive ion spectra of the three thiols (Figure 3), the low mass region (m/z < 100) is dominated by hydrocarbon fragments, presumably formed by fragmentation of the alkyl chain. Intense peaks are also observed at m/z 107 and 109, corresponding to elemental silver ions, reflecting the relative isotopic abundances of 52% and 48% for ^{107}Ag and ^{109}Ag. Above mass 110, a number of heavier fragments are observed that are dominated by silver and silver−sulfur species. These include the peaks due to Ag_2^+ (m/z 214, 216, and 218), Ag_2S^+ (m/z 246, 248, and 250), Ag_3^+ (m/z 321−327), Ag_3S^+ (m/z 353−359), Ag_5^+ (m/z 535−545), and Ag_5S^+ (m/z 567−577). Patterns of peaks are observed that clearly reflect the statistical distributions of clusters formed from the different isotopes of silver. For the larger fragments (especially Ag_4^+) the intensities of the observed peaks are weak. Besides these silver and silver−sulfur fragments, there are also three peaks that occur at m/z 135, 153, and 177 in all of the spectra, and two peaks that were observed intermittently at m/z 209/211. The identities of these peaks remain uncertain; they do not correspond to any common contaminants but are not obviously fragments of the adsorbate structure. Generally, however, there is an absence of peaks that contain fragments of the alkyl chain and S and/or Ag. There is one exception: the groups of peaks at m/z 359, 361, and 363 in the octanethiol spectrum, at m/z 415, 417, and 419 in the dodecanethiol spectrum, and at m/z 499, 501, and 503 in the ODT spectrum, which we suggest are due to $Ag_2(M-H)^+$ where M is the thiol molecular species.

Silver-adsorbate fragments are also observed in the negative ion spectra (Figure 4). Of particular importance are the peaks due to $Ag(M-H)S^-$ and $Ag(M-H)_2^-$, observed at m/z 284/286 and 397/399, respectively, for octanethiol, at m/z 340/342 and m/z 509/511, respectively, for dodecanethiol, and at m/z 424/426 and 677/679, respectively, for octadecanethiol. For dodecanethiol, $Ag(M-H)_2^-$ was more intense than $Ag(M-H)S^-$, while for octadecanethiol monolayers $Ag(M-H)S^-$ was slightly more intense than $Ag(M-H)_2^-$. We ascribe the difference in relative intensities here to the much higher mass of the $Ag(M-H)_2^-$ ion for octadecanethiol, meaning that more energy must be delivered to the desorption site in order for it to leave the surface. Consequently, the probability of emission of $Ag(M-H)S^-$ is increased in relative terms. However, the relative intensities of these peaks within the respective spectra remained constant as the time of exposure to the thiol solution was varied.

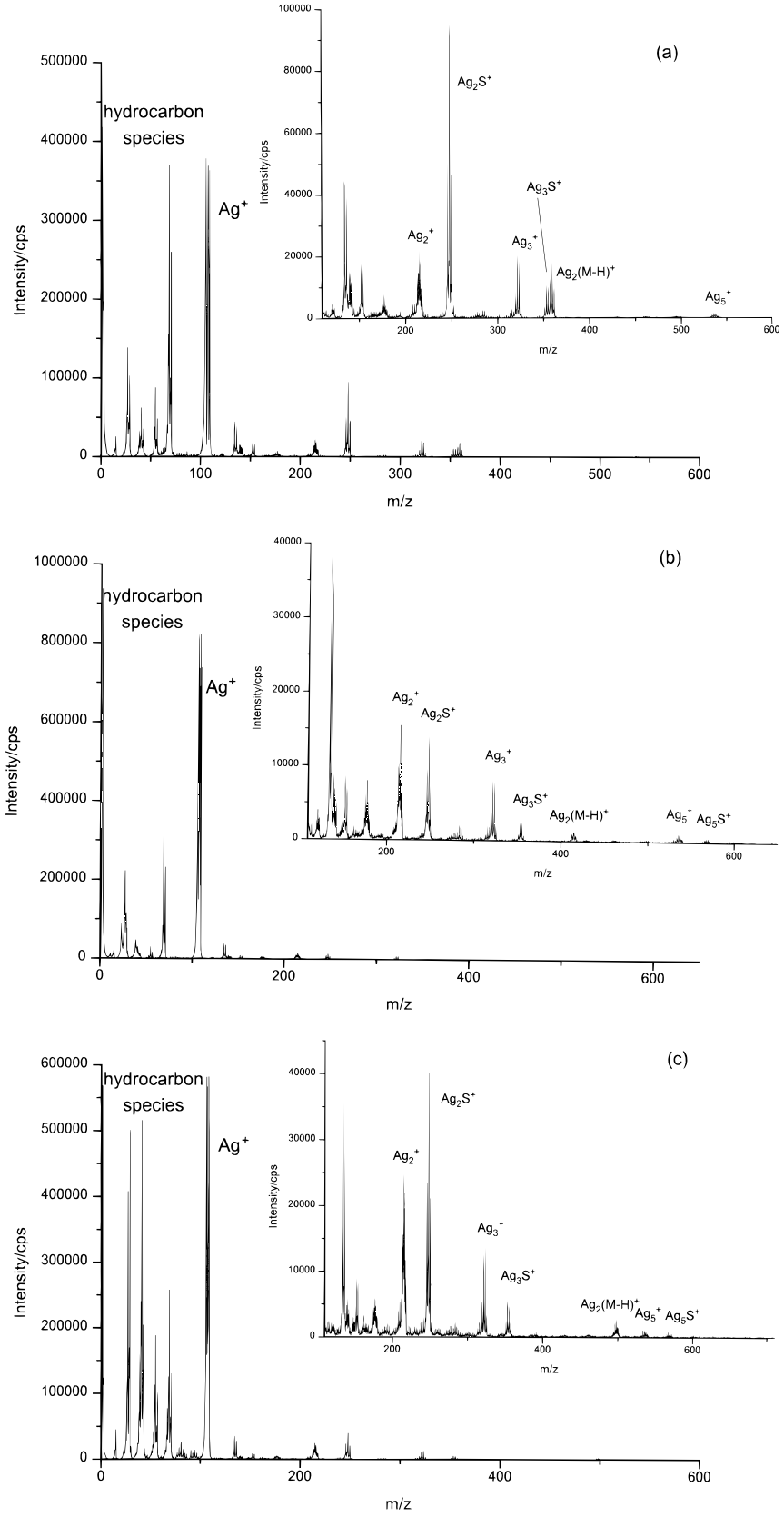

Figure 3. Positive ion SIMS spectra of (a) octanethiol, (b) dodecanethiol, and (c) octadecanethiol.

The spectra of all three SAMs exhibit prominent $[M-H]^-$ ions, at *m*/*z* 145 for octanethiol, at *m*/*z* 201 for dodecanethiol, and at *m*/*z* 285 for octadecanethiol. For all adsorption times, the $[M-H]^-$ peak is substantially larger than the $Ag(M-H)S^-$ peak. In addition, all of the spectra contain peaks at *m*/*z* 133, 171/3, 185/7, and 199/201, which remain difficult to identify. It is possible that the peaks at *m*/*z* 171/3, 185/7, and 199/201 correspond to AgS_2^-, $AgS_2CH_2^-$, and $[AgS_2C_2H_4]^-$, respectively. This would mean that they are fragments of the $Ag(M-H)S^-$ peak that only contain a small portion of the alkyl chain, thus explaining their appearance at the same *m*/*z* ratio in the spectra of all of the SAMs.

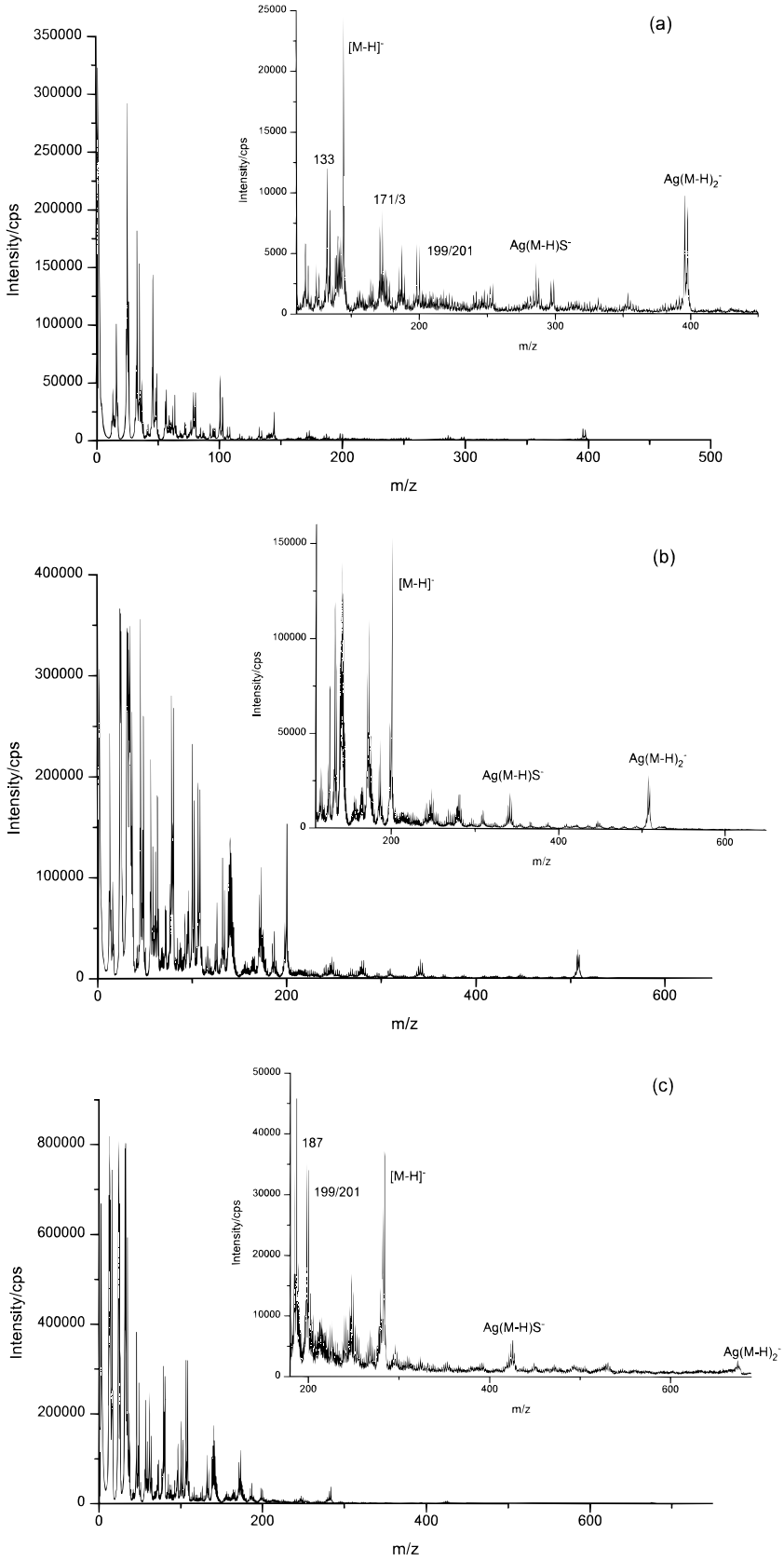

Figure 4. Negative ion SIMS spectra of (a) octanethiol, (b) dodecanethiol, and (c) octadecanethiol.

At lower *m*/*z* values (below *m*/*z* 100), the dominant peaks are due to elemental species or small fragments. CH^- is observed at *m*/*z* 13, O^- at *m*/*z* 16 (from trace contamination), C_2H^- at *m*/*z* 25, S^- at *m*/*z* 32, SH^- at *m*/*z* 33, and Cl^- at *m*/*z* 35/37, which is ubiquitous in negative ion SIMS spectra. A peak is observed at *m*/*z* 46, possibly due to SCH_2^-, and a number of other peaks are also observed that are common to the spectra of monolayers of all three thiols. Of particular interest is the region around *m*/*z* 80 and *m*/*z* 96. SO_3^- ions would appear at *m*/*z* 80 and SO_4^- ions at *m*/*z* 96. Peaks are observed at *m*/*z* 79 and 81 for freshly prepared SAMs of all of the thiols, for which no assignment can be made, and a small peak is sometimes

observed at *m*/*z* 80; however, the peak at *m*/*z* 80 was significantly less intense than the peaks at *m*/*z* 79 and 81 in almost all cases. A small peak is also observed at *m*/*z* 96 for the freshly prepared SAMs. SO_3^- and SO_4^- ions are frequently observed in negative ion SIMS spectra, often with high intensity. Trace contamination by oxysulfur species (not oxidized thiols) could thus give rise to significant peaks at *m*/*z* 80 and 96. In photooxidized monolayers (see below) the peak at *m*/*z* 80 rapidly becomes very much more intense than the peaks at *m*/*z* 79 and 81—much larger (relatively) than is the case for the freshly prepared SAMs. The small peaks occasionally observed at *m*/*z* 80 in the spectra of the freshly prepared monolayers are therefore not thought to be indicative of significant oxidation of the SAM.

Photooxidation of SAMs on Silver. XPS spectra obtained from SAMs of octanethiol and octadecanethiol as a function of photooxidation time are displayed in Figure 5. In agreement with our earlier study of the photooxidation of SAMs on gold,[20] a new feature develops at 167−168 eV in the S 2p region of the spectrum following UV exposure, attributed to SO_3 species. This peak grows in size with increasing irradiation time at the expense of the unoxidized component, while the O region shows an increased contribution at 532 eV, indicating the incorporation of O into the material. Figure 6 summarizes the extent of photooxidation by displaying the ratio of the SO_3 to (SO_3 + S) XPS peak areas from the S 2p data as a function of UV exposure time for each of the SAMs investigated. For the short-chain monolayers, there is a rapid increase in SO_3 up to 40 min UV exposure followed by a slower rate of O incorporation after this time. For the longer-chain SAMs, the rate of SO_3 production is lower than for hexanethiol and octanethiol even at short exposure times. In Figure 7 the O 1s/Ag $3d_{(5/2+7/2)}$ XPS peak area ratio is plotted for the photooxidation process and shows a generally linear increase in O content in the samples as a function of UV exposure time. Broadly speaking, these data indicate a chain-length dependence of the rate of photooxidation too, with hexanethiol SAMs exhibiting a faster rate of oxygen uptake than octadecanethiol (see the two lines fitted in Figure 7), although the chain-length dependence is less marked than in Figure 6. The C 1s/Ag $3d_{(5/2+7/2)}$ XPS peak area ratios are shown in Figure 8 as a function of UV exposure time for all the monolayers studied. Here again, there is a marked influence of alkyl chain length on the rate of change, with the SAMs formed from longer-chain molecules apparently losing large quantities of C during the photooxidation process, while for hexanethiol and octanethiol the C/Ag ratio appears unchanged.

In the static SIMS spectra of photooxidized SAMs, the most significant changes occur in the negative ion spectra (Figure 9). After only short exposures to UV radiation, a new peak appears that is attributed to the alkylsulfonate species. For octanethiol, this peak is observed at *m*/*z* 193, corresponding to $CH_3(CH_2)_7SO_3^-$ (hereafter, referred to as MSO_3^-). There is no peak, however, at *m*/*z* 209 (the *m*/*z* ratio of an alkyl sulfate species, MSO_4^-). The MSO_3^- peak grows with exposure, and the $[M-H]^-$ peak declines correspondingly. The MSO_3^- peak is completely absent from spectra of SAMs that have not been exposed to UV radiation. These ions provide a straightforward means by which the extent of photooxidation may be quantified from the SIMS data. Figure 10 shows the variation in the normalized intensity of the MSO_3^- peak relative to both the $[M-H]^-$ peak and the $Ag(M-H)_2^-$ peak in the spectra of photooxidized octanethiol. The $Ag(M-H)S^-$ and $Ag(M-H)_2^-$ peaks are significantly reduced in intensity in the spectra of the photooxidized SAMs—not only in absolute terms, but also relative to the intensity of the $[M-H]^-$ peak. It may be seen from Figure 10 that the $MSO_3^-/(MSO_3^- + Ag(M-H)_2^-)$ ratio reaches 1 more rapidly than the $MSO_3^-/(MSO_3^- + [M-H]^-)$ ratio, which changes more slowly as photooxidation proceeds. However, both suggest essentially compete photooxidation of the thiol species soon after 40 min exposure.

Elsewhere in the spectrum, there are further indicators of the rate and nature of the photooxidation process. A peak is observed to be very prominent at *m*/*z* 80 in the spectra of the photooxidized SAMs, even at short exposure times (see Figure 9), and remains a dominant peak in the spectra of samples subjected to longer exposure times. A small peak is also observed at *m*/*z* 96, due to sulfate, but this only becomes significantly intense in the spectra of samples subjected to fairly long exposure times and even then, it remains significantly less intense than the SO_3^- peak at *m*/*z* 80. Finally, we also observed a general reduction in the relative intensites of the S^- and HS^- ions in the spectra of photooxidized monolayers.

Discussion

The XPS data obtained for freshly prepared SAMs on silver are very similar to those obtained for SAMs on gold. The major point of interest is the discrepancy between our data and those of Laibinis et al.[8] for the effect of extended solution exposure on the quantity of S incorporated into the monolayers. Our work shows no increase in S content for increased adsorption time, while theirs shows an enormous rise over the same time period. However, the reason for this difference is unclear, since in all other respects the monolayers produced appear to be identical.

SIMS spectra of SAMs on silver have been reported previously by Gillen et al.,[17] who obtained negative ion spectra of mercaptoundecanoic acid monolayers that exhibited peaks due to Ag^-, AgS^-, AgS_2^-, Ag_2S^-, and $Ag_2S_2^-$. They also observed a peak at *m*/*z* 217, which they attributed to the $[M-H]^-$ ion. Our data also exhibit the silver−sulfur clusters reported by Gillen et al. and we have observed significant peaks due to $[M-H]^-$. However, they did not report observation of the $Ag(M-H)S^-$ and $Ag(M-H)_2^-$ peaks that we found to be prominent in the spectra of all three of the SAMs that we have studied.

The observation of an $Ag(M-H)_2^-$ ion in the SIMS spectra of SAMs on Ag may be interpreted in a variety of ways. Related species have also been observed in SIMS spectra of SAMs on Au. Leggett et al.[25] reported a variety of fragments of the type Au_xM_y and Au_xS_y in spectra of 3-mercaptopropanoic acid on gold, while Tarlov and Newman[26] commented on the observation of $Au[M-H]_2^-$ species in their study of a variety of thiol monolayers on Au. They suggested that if thiol adsorption was predominantly onto 3-fold hollow sites, then the formation of such species by direct emission was unlikely; instead, recombinative processes may occur above the solid surface. Alternatively, they also suggested that such species may arise from defect sites. Consideration of Fenter's model[2] for the structure of octadecanethiol on Au leads to a further alternative explanation. On the basis of X-ray diffraction data, Fenter et al. suggested that octadecanethiol adsorbs onto Au(111) to form disulfides in which the alkyl chains nevertheless adopt a $(\sqrt{3} \times \sqrt{3})R30°$ lattice. The observation of $Au[M-H]_2^-$ species would then simply be a reflection of the nature of the bonding of the adsorbate at the surface. However, although there is some additional support for Fenter's model, it is not unequivocal and, furthermore, such models may not apply to SAMs on Ag because of the different headgroup/substrate

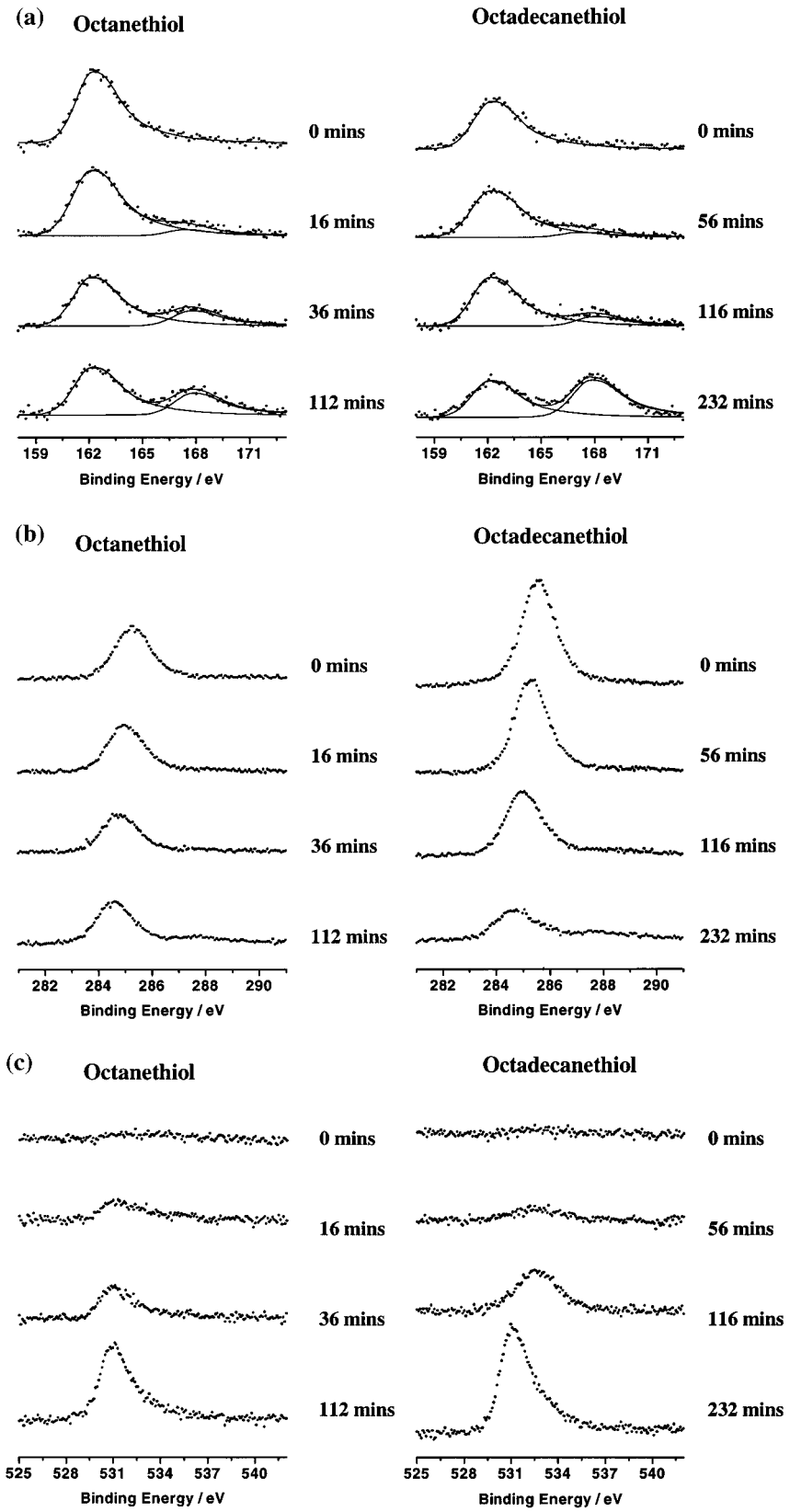

Figure 5. XPS spectra obtained from SAMs of octanethiol and octadecanethiol on silver as a function of UV photooxidation time: (a) S $2p_{(3/2,1/2)}$, (b) C 1s, and (c) O 1s regions.

interactions that are expected to arise from the Ag−S bond. Although our understanding of the S−Au interaction in SAMs (on Au) is poor, there is even less evidence for the structures of SAMs on silver. Although both diffraction studies[2] and scanning tunneling microscopy (STM) studies[3,4] suggest that the alkyl chains adopt a hexagonal arrangement, there are no clear indications regarding the arrangement of the sulfur atoms. Thus, it is difficult to read significance into the observation of either $Au[M-H]_2^-$ ions or $Ag[M-H]_2^-$ ions in the SIMS spectra. Our understanding of the nature of the S-metal interaction is not sufficiently well developed to facilitate a reliable conclusion.

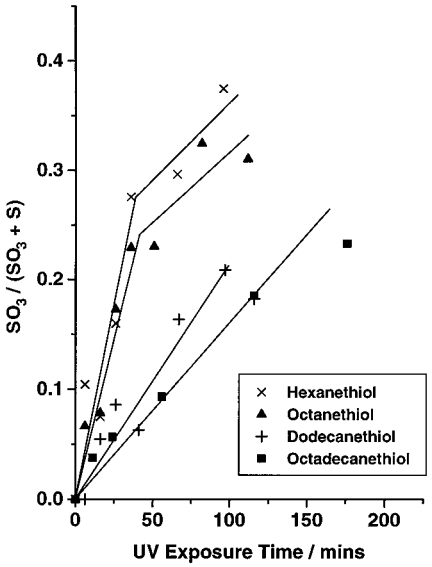

Figure 6. S $2p_{(3/2,1/2)}$ XPS peak area ratios for oxidized (SO_3) and unoxidized (S) components expressed as $SO_3/(SO_3 + S)$ as a function of UV exposure time for each of the monolayers studied. The lines are drawn to guide the eye and are not the result of rigorous fitting of the data.

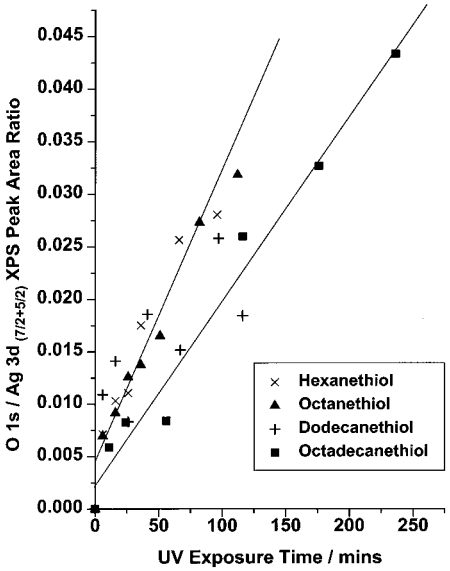

Figure 7. O 1s/Ag $3d_{(7/2,5/2)}$ XPS peak area ratios as a function of UV exposure time and monolayer chain length.

Gillen et al.[17] used imaging SIMS to examine SAMs that had been photooxidized by exposure to UV light through a mask. They found that the HS^- signal was significantly reduced in the images of oxidized SAMs and could be used to map the distribution of unoxidized material, while strong HSO_4^- signals could be used to map the distribution of oxidized material. They reported contrast ratios (light to dark areas) of 10:1 and 15:1 for the SH^- and HSO_4^- images, respectively. In our studies, we have also found that the HS^- signal declines with exposure to UV light; however, it does not appear to do so in a way that could be straightforwardly quantified. It is difficult to be clear which peak it could be referenced against, for there are no other peaks in the low mass region of the negative ion SIMS spectrum, save the SO_3^- peak, that exhibit clear UV exposure-dependent trends. Our data suggest that the intensities of the HSO_4^- peak (*m*/*z* 97) and the SO_4^- peak (*m*/*z* 96) would not be a completely reliable guide to the extent of photooxidation. Although both

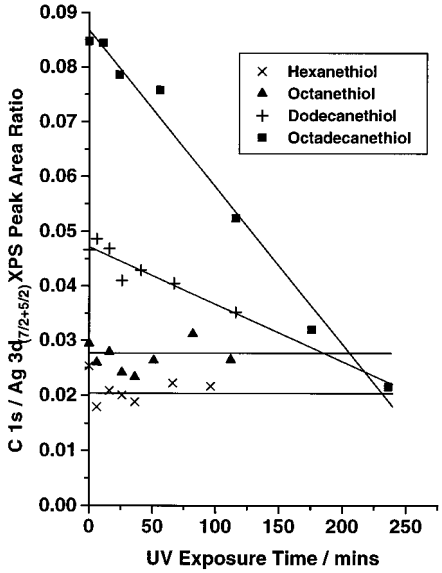

Figure 8. C 1s/Ag $3d_{(7/2,5/2)}$ XPS peak area ratio as a function of UV exposure time for all the monolayers studied.

do appear to increase with increasing UV irradiation time, the extent of the change is variable and, moreover, both peaks are also observed in the spectra of unoxidized SAMs as a consequence of the presence of trace quantities of contaminants. The MSO_3^- peak provides a much more specific indication of the extent of SAM photooxidation; it is absent from the spectra of monolayers that have not been exposed to UV radiation and shows a clear dependence on the time of exposure. Furthermore, variations in the intensity of the $[M-H]^-$ peak also provide corroboration of the trends observed in the intensity of the MSO_3^- peak: as the MSO_3^- peak increases, the $[M-H]^-$ peak declines in intensity. By monitoring the variation in the $MSO_3^-/([M-H]^- + MSO_3^-)$ ratio (Figure 10), we have been able to accurately quantify the extent of photooxidation of the SAMs and to make correlations between the SIMS and XPS data.

The XPS ratios displayed in Figure 6 show that there appears to be a chain length dependence of the rate of photooxidation, as was observed for SAMs on gold, with SAMs of long-chain molecules taking much longer than short-chain ones to produce the same degree of reaction. However, compared to gold, the rate of photooxidation initially appears to be much slower on Ag, with approximately only a third of the S oxidized after 40 min exposure, a time period over which complete oxidation of octanethiol on gold occurred. Further analysis of the data indicates that the mechanism is somewhat different for the two systems. In the SIMS ratio data in Figure 10 it can be seen quite clearly that after 40 min photooxidation the amount of $(M-H)^-$ and $Ag(M-H)_2^-$ species produced in the spectra has decreased to approximately zero, indicating that the amounts of unoxidized thiol species at the surface have correspondingly decayed to zero as well. In contrast, the $SO_3/(SO_3 + S)$ ratio obtained from the XPS data in Figure 6 shows that only 0.25−0.3 of the total surface S has been oxidized at this point. The total quantity of S present at the surface during photooxidation did not change for any of the SAMs, however, indicating that the data are not complicated by desorption of significant quantities of S-containing species. Furthermore, this implies that the oxidized species are still held at the surface, presumably because of the stronger SO_3−Ag interaction, in contrast to the situation on gold where significant desorption of the alkylsulfonates occurred. After approximately 40 min photooxidation, the rate of change of the $SO_3/(SO_3 + S)$ XPS ratio decreased

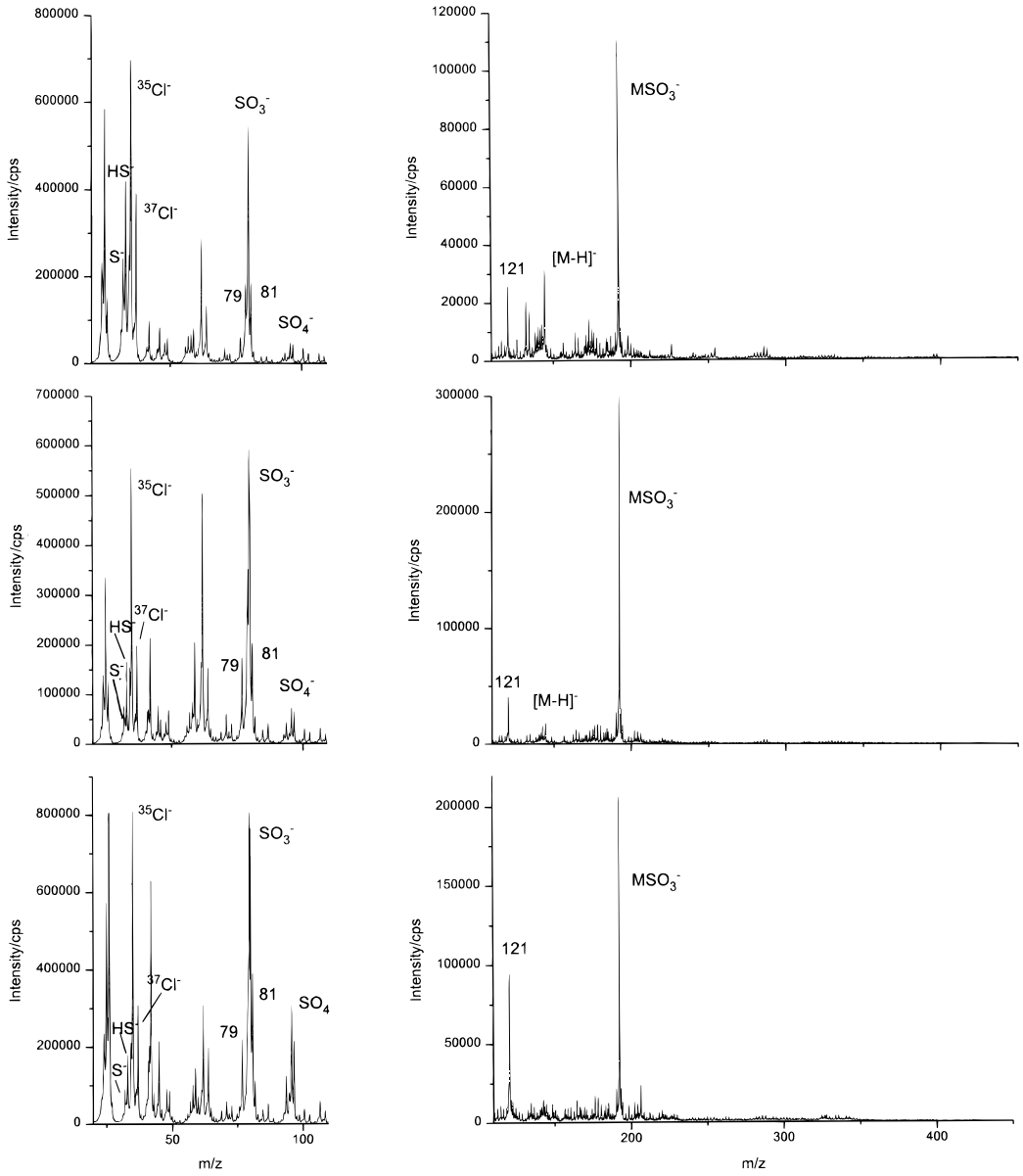

Figure 9. Development of two key regions of the negative ion SIMS spectrum of octanethiol as a function of time of exposure to the UV source. Exposure times are 16 min (top), 36 min (center), and 116 min (bottom).

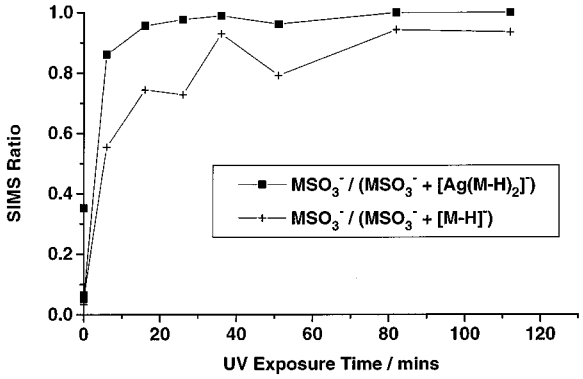

Figure 10. Plot of the $MSO_3^-/(MSO_3^- + [M-H]^-)$ and $MSO_3^-/(MSO_3^- + Ag(M-H)_2^-)$ SIMS ion intensity ratios as a function of UV exposure time for octanethiol.

for hexanethiol and octanethiol, implying the slower oxidation of the remaining S (presumably due to its different nature). This would require a large quantity of S at the surface on formation of the SAM that is not bound to an alkyl chain. This could occur either from the formation of a silver sulfide interlayer as suggested by Laibinis et al. or as a consequence of the presence within the monolayer of a significant number of molecules that have undergone S−C bond scission, with the alkyl components remaining held in place by interchain van der Waals interactions.

To test whether our data were consistent with first-order kinetics, the natural logarithm of the $(SO_3)/(SO_3 + S)$ ratio shown in Figure 6 was plotted against exposure time. Linear regression yielded a poor fit to a straight line for these data, indicating that a first-order mechanism probably does not apply. The detailed kinetics of the photooxidation process thus require further investigation. In contrast, our data for the photooxidation of SAMs on Au fitted a simple first-order scheme,[20] adding weight to the conclusion above that the mechanisms of photooxidation of SAMs on Ag and Au are different.

In an earlier study, Lewis et al.[21] recorded surface-enhanced Raman (SER) spectra of photooxidized monolayers of hexanethiol on Ag. They attributed a weak shoulder at 917 cm^{-1} and a peak at 606 cm^{-1} to sulfite species but attributed peaks at 460, 618, and 1132 cm^{-1} to sulfate species. The observation

of an MSO_3^- ion in our work provides definitive confirmation that photooxidation of thiol SAMs on Ag leads to the formation of sulfonate species. Our SIMS spectra do suggest that inorganic sulfate species are produced by photooxidation; however, these are not the dominant oxysulfur species in the low mass region of the SIMS spectrum. Moreover, the observation of alkylsulfonates as the sole organic oxysulfur species suggests that the sulfates in the oxidized materials are not produced directly from the adsorbate. We speculate that the sulfates are formed at high UV exposures, probably from inorganic sulfur species produced by the action of UV light. This is consistent with the fact that static SIMS spectra do not exhibit significant SO_4^- peaks until exposure times that are longer than those required for complete oxidation of the monolayer (see Figure 9). The amounts of sulfate species produced are likely to be small over the UV exposures required to photooxidize the thiol headgroups, however, since the XPS data for the S 2p region (Figure 5) do not exhibit a component due to SO_4. Although the S 2p spectra are noisy, the presence of significant quantities of sulfates should lead to a feature some 2.5 eV to the high binding energy side of the sulfonate feature.[27] The observation of sulfates by Lewis et al. may reflect differences in the emission of their lamp (for example, it may yield a greater power, leading to more extensive oxidation of inorganic sulfur species, or may produce emission over a different range of wavelengths).

Lewis et al. postulated that the mechanism of SAM photooxidation on Ag involved initial S−C bond cleavage followed by desorption of alkyl fragments and oxidation of surface-bound sulfur species. Such a mechanism is consistent with our data, which suggest that significant quantities of inorganic sulfur are produced during photoirradiation of SAMs on Ag and are apparently much more slowly oxidized than residual intact thiol molecules, although this is clearly not the sole process because a significant fraction of the adsorbate molecules are oxidized to yield alkylsulfonates. In previous studies in this laboratory,[20] we used XPS to monitor the photooxidation of SAMs on Au and found that the rate of photooxidation exhibited a pronounced dependence on alkyl chain length. We concluded that the rate-determining step was the penetration of oxygen species to the Au/S interface, whereupon rapid oxidation to yield the alkylsulfonate occurred. We speculated that a different mechanism may occur for SAMs on silver, explaining the apparent difference between our mechanism and that of Lewis et al. The data presented here provide strong support for this hypothesis.

In conclusion, we are able to suggest a photooxidation mechanism for SAMs on Ag in which two competing processes are taking place. The first involves the photooxidation of alkylthiolates to alkylsulfonates. For this process, the rate shows a similar dependence on the alkyl chain length to that observed for SAMs on gold as a result of steric constraints on the penetration of the reactive species to the S−Ag interface. The second process involves S−C bond scission induced by UV light and leads to an increase in the amount of inorganic S at the surface. This inorganic S oxidizes more slowly and, based on the observations of Lewis et al., may ultimately form SO_4 species. For longer-chain molecules the first process is slower and XPS indicates a larger fraction of inorganic S at the surface. The importance of S−C bond scission and the extent of production of inorganic S during the photoirradiation of SAMs on silver constitute a significant difference from the mechanism that applies to SAMs on gold substrates. However, the residual inorganic sulfur species apparently present no obstacle to the use of photopatterned SAMs for the microfabrication of silver structures. Studies in the authors' laboratory have shown that they may be effectively employed, in combination with wet etching processes, to create micrometer-scale structures.

Finally, it remains unclear which wavelength is responsible for the photooxidation of SAMs on silver and on Au. Further studies may furnish a more detailed understanding of the mechanism of SAM photooxidation on both gold and silver. Such studies may lead not only to improved microfabrication methodologies but also, by comparison of the behavior of SAMs formed on the two different metals, to an enhanced understanding of the role of substrate−adsorbate interactions in governing the properties and reactivity of SAMs more generally.

Conclusion

SAMs on silver have been characterized using XPS and static SIMS. XPS data indicate that the composition of the monolayers, and in particular the sulfur content, is not dependent on the time of exposure to the thiol solution, in contrast to results published by other workers. Static SIMS spectra exhibit a number of molecular species that contain intact adsorbate molecules. No significant changes are observed in the relative intensities of these species as a function of the time of exposure to the thiol solution, in agreement with the XPS data. SAMs on Ag are photooxidized to yield alkylsulfonate species as the sole organic oxidation product. However, scission of the S−C bond is also an important process—perhaps the more important of the two in some cases—leading to the formation of alkyl fragments that remain bound within the monolayer by van der Waals interactions. S−C bond scission leads to the formation of inorganic sulfur, which is oxidized to yield inorganic sulfur oxidation products. Static SIMS proved to be highly sensitive to changes in the molecular structure of the molecules that formed the SAMs and allowed the quantification of the rate of oxidation of thiol headgroups specifically, while XPS only revealed the total amount of oxidized sulfur.

Acknowledgment. The authors are grateful to the EPSRC (Grant GR/K/28671) and the Leverhulme Trust (Grant F114AY) for financial support for this work.

References and Notes

(1) Laibinis, P. E.; Fox, M. A.; Folkers, J. P.; Whitesides, G. M. *Langmuir* **1991**, *7*, 3167.
(2) Fenter, P.; Eisenberger, P.; Li, J.; Camillone, N.; Bernasek, S.; Scoles, G.; Ramanarayanan, T. A.; Liang, K. S. *Langmuir* **1991**, *7*, 2013.
(3) Dhirani, A.; Hines, M. A.; Fisher, A. J.; Ismail, O.; Guyot-Sionnest, P. *Langmuir* **1995**, *11*, 2609.
(4) Heinz, R.; Rabe, J. P. *Langmuir* **1995**, *11*, 506.
(5) Camillone, N.; Chidsey, C. E. D.; Liu, G.; Scoles, G. *J. Chem. Phys.* **1993**, *98*, 3503.
(6) Delamarche, E.; Michel, B.; Gerber, Ch.; Anselmetti, D.; Guntherodt, H.-J.; Wolf, H.; Ringsdorf, H. *Langmuir* **1994**, *10*, 2869.
(7) Poirier, G. E.; Tarlov, M. J. *Langmuir* **1994**, *10*, 2853.
(8) Laibinis, P. E.; Whitesides, G. M.; Allara, D. L.; Tao, Y.-T.; Parikh, A. N.; Nuzzo, R. G. *J. Am. Chem. Soc.* **1991**, *113*, 7152.
(9) Laibinis, P. E.; Bain, C. D.; Nuzzo, R. G.; Whitesides, G. M. *J. Phys. Chem.* **1995**, *99*, 7663.
(10) Mrksich, M.; Whitesides, G. M. *Trends Biotechnol.* **1995**, *13*, 228.
(11) Wilbur, J. L.; Kumar, A.; Kim, E.; Whitesides, G. M. *Adv. Mater.* **1994**, *6*, 600.
(12) Xia, Y.; Kim, E.; Whitesides, G. M. *J. Electrochem. Soc.* **1996**, *143*, 1070.
(13) Kumar, A.; Biebuyck, H. A.; Whitesides, G. M. *Langmuir* **1994**, *10*, 1498.
(14) Abbott, N. L.; Rolison, D. R.; Whitesides, G. M. *Langmuir* **1994**, *10*, 2672.

(15) Huang, J.; Dahlgren, D. A.; Hemminger, J. C. *Langmuir* **1994**, *10*, 626.
(16) Tarlov, M. J.; Burgess, D. R. F.; Gillen, G. *J. Am. Chem. Soc.* **1993**, *115*, 5305.
(17) Gillen, G.; Bennett, J.; Tarlov, M. J.; Burgess, D. R. F. *Anal. Chem.* **1994**, *66*, 2170.
(18) Cooper, E.; Wiggs, R.; Hutt, D. A.; Parker, L.; Leggett, G. J.; Parker, T. L. *J. Mater. Chem.* **1997**, *7*, 435.
(19) Huang, J.; Hemminger, J. C. *J. Am. Chem. Soc.* **1993**, *115*, 3342.
(20) Hutt, D. A.; Leggett, G. J. *J. Phys. Chem.* **1996**, *100*, 6657.
(21) Lewis, M.; Tarlov, M. J.; Carron, K. *J. Am. Chem. Soc.* **1995**, *117*, 9574.
(22) Caution: Piranha solution may detonate spontaneously on contact with organic material.
(23) Bain, C. D.; Troughton, E. B.; Tao, Y.-T.; Evall, J.; Whitesides, G. M.; Nuzzo, R. G. *J. Am. Chem. Soc.* **1989**, *111*, 321.
(24) The two components of the S 2p XPS peak ($^1/_2$ and $^3/_2$) are separated by only 1 eV and therefore have not been resolved by our system using a 50 eV pass energy to maximize sensitivity.
(25) Leggett, G. J.; Davies, M. C.; Jackson, D. E.; Tendler, S. J. B. *J. Phys. Chem.* **1993**, *97*, 5348.
(26) Tarlov, M. J.; Newman, J. G. *Langmuir* **1992**, *8*, 1398.
(27) *Auger and X-ray Photoelectron Spectroscopy*; Briggs, D., Seah, M. P., Eds.; Practical Surface Analysis 1; Wiley: Chichester, 1990; p 604.